The mechanosensitive protein Vinculin organizes actomyosin and maintains epithelial tricellular junctions

Jolene Iseler

March 31, 2023

This thesis has been read and approved by Dr. Ann L. Miller

Signed: _____ Date: ____ / ____ / _____

Faculty advisor email: annlm@umich.edu Phone: (734)-764-9732

Table of Contents

Acknowledgements

First, I would like to thank my principal investigator and mentor **Dr. Ann Miller** for her guidance and for the example she has set. I am consistently in awe of her commitment to the lab while still maintaining a healthy work-life balance. Her attention to detail is admirable and has helped me become a better scientist. The way in which she cultivates a fun, open, and communicative work environment is something that I'd like to take to my next job.

Next, I would like to thank my graduate student mentor, **Lotte van den Goor**, whom I work with most directly in the lab. I am incredibly grateful for the training and advice you have given me, but above all, I must thank you for two things: showing me what excellence in mentoring looks like and encouraging me to pursue my goal of going to graduate school. I strive to have your patience while mentoring and your clarity in explaining science. You have made my experience in the lab so positive that I have decided to continue working in science through graduate school.

Many thanks are due to all my **fellow Miller lab members**, past and present, for making the lab environment such a fun and uplifting place to be: Zie, Anna, Kelsey, Jen, Rachel, Babli, Mitchell, Parker, Alex, Sara, Shahana, Katherine, and Claire. I will forever remember our memories made during spirit week. There are no other people with which I would rather celebrate a triumph or laugh over a blunder.

I'd like to thank **Judy Beam** for encouraging me to apply to the University of Michigan while I was in high school. I am grateful for her interest in guiding future generations of scholars and for believing in me.

To all **my friends**: college was made not only bearable, but enjoyable because of you. We have spent so much time together that I will never forget. In particular, I'd like to thank Jane and Autumn for their friendship. Talking with you two always makes my academic problems seem manageable. You both have helped me grow as a person during the past four years, and I hope to continue to watch you grow in upcoming years.

I'd like to thank **Dr. Josie Clowney** and **Dr. Anthony Vecchiarelli** for reading my senior thesis. I appreciate the time you set aside to read this, and your feedback will help me grow as an academic.

In addition, I'd like to thank **my brother** and **my sister**. To my brother Maxwell, you are the best brother I could ask for. I'll always aspire to have your multitalented creative nature. For now and forever, I love you and am proud of you. To my sister Justine, thank you for teaching me to be assertive and always stand my ground. I know that I will always have you in my corner, and you will always have me in yours. Thank you both for supporting me and listening to me while I worked towards my degree.

Finally, I am most thankful to **my mother**. For all that you have sacrificed to raise me, I hope to make you proud in return. I could not have achieved a fraction of what I have without your support and care. Thank you for being a champion for yourself and for our family. I am immensely grateful for the lessons you have taught me. I do it all for you.

Thank you to everyone who has played a part in supporting me during this project and during my time at the University of Michigan.

Abstract

Epithelial cells form barriers that coat and protect organs and organisms from their environments. Epithelial tissue function requires both adherens junctions to adhere cells together and tight junctions to create a selectively permeable barrier between neighboring cells. Sites of high tension along cell-cell contacts are called tricellular junctions, the points where three cells meet. Junctional integrity must be maintained when epithelia are challenged by mechanical stress, such as food passing through the intestines or the bladder expanding. Vinculin, a mechanosensitive protein, strengthens adherens junctions in response to mechanical stress through increasing connections to an actomyosin (F-actin and Myosin II) array.

Here, we aimed to characterize how Vinculin, actomyosin, and junctional proteins are reorganized at tricellular junctions after either Vinculin knockdown and/or the tension-increasing treatments. We began by quantifying changes in fluorescence intensity of mNeon-Vinculin and Halo-Vinculin at tricellular junctions after increasing tension in the epithelia. After ATP treatment or the optogenetic activation of RhoA, we found that Vinculin intensity is enriched at tricellular junctions and reorganizes from distinct "spots" into elongated "spokes" along the junction. To understand Vinculin's effects in maintaining actomyosin, we performed immunofluorescence staining for F-actin and Myosin II light chain in control and Vinculin knockdown epithelia. We found that there are reduced levels of actomyosin and disrupted actomyosin organization at tricellular junctions when Vinculin is knocked down. Next, we aimed to investigate whether Vinculin supports tricellular junction integrity. To test this, we performed immunofluorescence imaging of the adherens junction protein E-cadherin and the tricellular tight junction protein Angulin-1 after Vinculin knockdown. These experiments show that Vinculin knockdown decreases E-cadherin and Angulin-1 intensity at tricellular junctions, suggesting that Vinculin plays a role in maintaining tricellular adherens and tight junctions. Finally, to explore Vinculin's role in barrier function, we performed a barrier assay, ZnUMBA, to measure leaks in the space between cells. With this assay, we found a greater percentage of leaky tricellular tight junctions under Vinculin knockdown conditions. Taken together, these data suggest that the mechanosensitive recruitment of Vinculin to tricellular adherens

junctions under increased tension is essential for proper actomyosin organization and maintaining junctional integrity.

Introduction

i. Introduction to Epithelial Cells

Sheets of epithelial cells separate different compartments of our bodies and protect us from external pathogens (Marchiando et al., 2010). For example, epithelia make up our skin as well as the linings of our intestines and our lungs. Cell-cell junctions connect epithelial cells: tight junctions (TJs) selectively control the passage of material in the space between cells (the paracellular space) and adherens junctions (AJs) attach neighboring cells to each other and mechanically integrate them into the epithelial tissue. Both types of junctions are linked to a belt of actin and myosin (actomyosin) located at the apical side of the cell (Arnold et al., 2017; Hartsock & Nelson, 2008). There are many aspects that regulate the state of junctional actomyosin, but a key regulator of actin dynamics is the family of Rho GTPases, specifically RhoA GTPase (Agarwal & Zaidel-Bar, 2019). GTP-bound RhoA acts on its effector proteins, such as formin, which promotes assembly of long unbranched actin filaments, and Rho-associated coiled-coil kinase (ROCK), which phosphorylates and activates Myosin II to drive contractility at cell-cell junctions (Arnold et al., 2017). To maintain cell-cell adhesion, such cytoskeleton and cytoskeleton-associated proteins must work to generate and transmit tension from various cellular and tissue-scale forces acting at junctions, such as cell division, cell extrusion, and collective cell migration (Mao & Baum, 2015).

ii. Tight Junctions

TJs are located most apically in vertebrate epithelial cells and are composed of strands of transmembrane claudins and Occludin that seal the paracellular space (Otani & Furuse, 2020). TJs are connected to the actin cytoskeleton via the zonula occludens (ZO) family of proteins (Otani & Furuse, 2020).

iii. Adherens Junctions

AJs function to mechanically couple neighboring cells and are located basally to TJs. Like TJs, AJs consist of transmembrane proteins and cytosolic linker proteins that connect AJs to the actin cytoskeleton. E-cadherin, a transmembrane protein, interacts with E-cadherins on neighboring cells to join AJs to one another (Hartsock & Nelson, 2008). E-cadherin binds directly to the cytosolic linker protein ß-catenin, which in turn binds to α-catenin (Mege & Ishiyama, 2017). α-catenin is a mechanosensitive intracellular protein that connects AJs to the actin cytoskeleton (Mege & Ishiyama, 2017; Yonemura, 2011a). Upon increased tension, α-catenin adopts an open conformation which reveals a binding site for Vinculin (Mege & Ishiyama, 2017; Seddiki et al., 2018).

iv. The Mechanosensitive Protein Vinculin

Vinculin is a mechanosensitive protein that is relatively newly recognized to localize to epithelial AJs (Bays & DeMali, 2017). Mechanosensitivity is the term used to describe the ability of a cell to sense mechanical stimuli and convert that into cellular changes (Yonemura, 2011b). Previous literature has outlined Vinculin's mechanosensitive properties at cell-substrate adhesions, where Vinculin is recruited in a force-dependent manner (Atherton et al., 2016). Composed of head, linker, and tail domains, Vinculin is a 116 kDa protein that links junctional α-catenin with the actin cytoskeleton (Janssen et al., 2006). Vinculin exists in an auto-inhibited form or an open form based on its ligand-binding and phosphorylation state (Bays et al., 2014; Ziegler et al., 2006). Vinculin has a prominent role at cell-substrate adhesions, and its binding partners have been well-characterized there (Bays & DeMali, 2017). However, less is known about Vinculin's role in cell-cell adhesions (Bays & DeMali, 2017). Recent work has shown that Vinculin is recruited to sites of increased tension at cell-cell junctions, specifically the cytokinetic cleavage furrow, to reinforce the connection of AJs to the cytoskeleton (Higashi et al., 2016). While Vinculin has been studied in the context of cell-substrate adhesions and bicellular junctions, its role specifically at tricellular junctions is not well understood.

v. Tricellular Junctions

Tricellular junctions (TCJs), including both tricellular tight junctions (tTJs) and tricellular adherens junctions (tAJs), are specialized junction structures that form where three cells meet. TCJs are sites of increased tension due to actomyosin-generated contractility along each edge of the junction (Higashi & Miller, 2017; Trichas et al., 2012). Two proteins that localize uniquely to tTJs are the angulins, a family of three single-pass transmembrane protein with tissue-specific expression patterns, and Tricellulin, a four-pass transmembrane protein that interacts with actomyosin and is related to Occludin (Cho et al., 2022; Sugawara et al., 2020). Like bicellular TJs, tTJs also function to seal the paracellular space and regulate barrier function, as loss of either angulin or Tricellulin negatively affects barrier function (Higashi & Miller, 2017). Afadin, a cytoplasmic protein, and Sidekick, a single-pass transmembrane protein, are two proteins enriched at tAJs, which are recruited to TCJs in a tension-dependent manner (Manning et al., 2019; Yu & Zallen, 2020). Despite the recent strides that have been made in investigating TCJs, there are still many gaps in our understanding of how actomyosin is coupled to these junctions and how tension is transmitted between TCJs to the cytoskeleton.

Prior work from the Miller lab focused on Vinculin's role in strengthening the AJ at cleavage furrows of dividing cells, but also revealed that Vinculin accumulates strongly at TCJs (Higashi et al., 2016; Higashi & Miller, 2017). Here, we build on that finding by investigating Vinculin's role at TCJs. We hypothesized that Vinculin is required at TCJs for proper tAJ/tTJ architecture and tension transmission.

Results

i. **Vinculin is mechanosensitively recruited to tricellular junctions**

To investigate how Vinculin supports TCJ integrity, we use the animal cap epithelial cells of *Xenopus laevis* embryos as a model system because they are excellent for both live and fixed imaging. Additionally, the junctional proteins and ultrastructure of cell-cell junctions are well conserved with that of humans; indeed, *X. laevis* Vinculin has high sequence homology (90% identity) with human Vinculin. By knocking down Vinculin using a specific morpholino oligo (MO) that binds to the 5' untranslated region of endogenous Vinculin mRNA and blocks its translation, thus reducing levels of endogenous Vinculin in the cell, we characterize Vinculin's role in organizing the actomyosin array in epithelial cells and maintaining tTJs and tAJs.

First, we tested if Vinculin's mechanosensitive property would allow it to be recruited to TCJs under tension. To explore Vinculin's recruitment to TCJs, we used two methods to increase tension in the epithelium: the optogenetic activation of RhoA GTPase and the addition of extracellular ATP (**Figure 1A**). For the optogenetic activation of RhoA, we adapted the TULIP optogenetic system for use in *X. laevis*. We inject the *X. laevis* embryos with mRNA constructs for a photorecruitable GEF (prGEF) and a plasma membrane anchoring protein fused to the photosensitive LOVpep domain. Upon blue light (405 nm) stimulation, the photorecruitable GEF gets recruited to the plasma membrane where it can activate RhoA (**Figure 1B**) (Strickland et al., 2012; Varadarajan et al., 2022). For the extracellular ATP addition, we pipette a solution of 500 μM ATP onto the slide with the *X. laevis* embryo, and contraction occurs within the epithelia (Arnold et al., 2019; Joshi et al., 2010; Kim et al., 2014) (**Figure 1C**). In both cases, we imaged live *X. laevis* embryos at gastrula stage (Nieuwkoop and Faber stage 10-11) because they have formed a polarized epithelia with polarized AJs and TJs by this stage (Barua et al., 2021).

Imaging fluorescently-tagged Vinculin constructs (Halo-Vinculin+JaneliaFluor 646 and mNeon-Vinculin) in the epithelia reveals that Vinculin is present at TCJs at baseline tension. Fluorescently tagged Vinculin is then enriched at TCJs under increased tension from both the optogenetic activation of RhoA

(**Figure 1D**) and the extracellular addition of ATP (**Figure 1F**), and quantification of fluorescently-tagged Vinculin intensity at TCJs demonstrates this (**Figure 1E and 1G)**. Interestingly, when comparing results between the two tension-increasing methods, the optogenetic activation of RhoA seems to cause a stronger accumulation of fluorescently-tagged Vinculin at TCJs than the addition of extracellular ATP. We believe that differences in the way tension is generated in these two methods can explain this outcome. Because the photorecruitable GEF is recruited to the plasma membrane, we believe tension is being generated parallel to and near the plasma membrane. The exact mechanism by which adding extracellular ATP generates tension is unknown, but it has been demonstrated that the addition of extracellular ATP increases tension in *X. laevis*, and that adding ATP increase the amount of medial-apical F-actin fluorescence intensity (Arnold et al., 2019; Kim et al., 2014). We hypothesize that tension is being generated in the medial-apical area of the cell (as opposed to junctional tension) when extracellular ATP is added. Further supporting this explanation, our results that show that upon ATP addition, apical cell-cell junctions generally become "wavy", perhaps from a population of medial-apical actin pulling inwards, whereas optogenetic stimulation generally makes cell-cell junctions appear more "taut" from actomyosin contracting parallel to cell-cell junctions (data not shown).

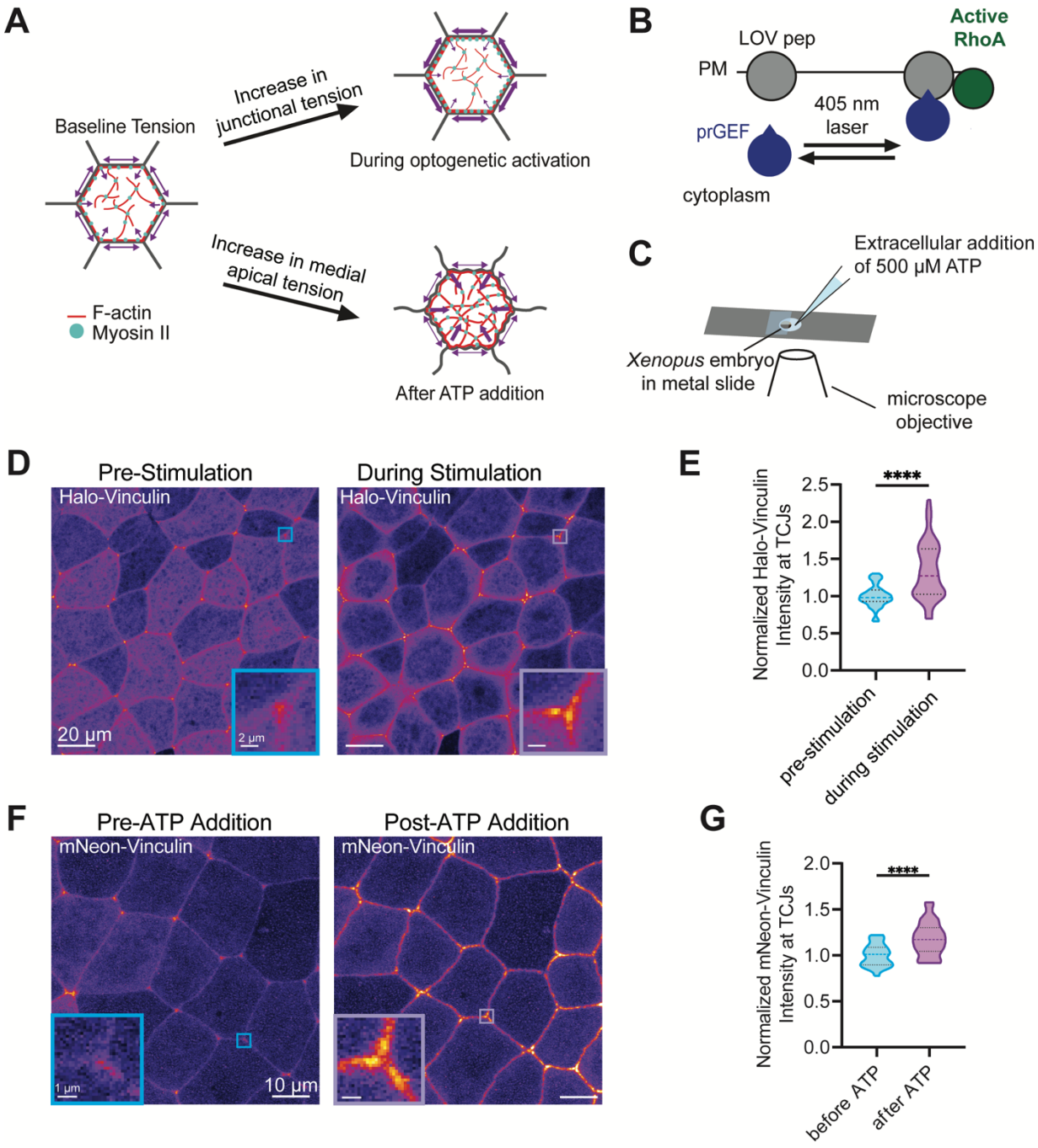

Figure 1: Vinculin is mechanosensitively recruited to tricellular junctions.
(A) Diagram of increase in tension through the optogenetic activation of RhoA and through the addition of extracellular ATP. **(B)** Experimental setup of the optogenetic activation of RhoA. **(C)** Experimental setup of the addition of extracellular ATP. **(D)** *En face* view of Halo-Vinculin's (with Janelia Fluor 646 dye) mechanosensitive recruitment to TCJs through the optogenetic activation of RhoA. **(E)** Quantification of TCJ Halo-Vinculin fluorescence intensity before and during optogenetic stimulation. Statistics, paired t-test; n = 3 experiments, 9 embryos, 55 TCJs; $p \leq 0.0001$ (****). Violin plots show the median (dashed line) and the 25th and 75th quartiles (dotted lines). **(F)** *En face* view of mNeon-Vinculin's mechanosensitive recruitment to TCJs through the addition of extracellular ATP. **(G)** Quantification of TCJ mNeon-Vinculin fluorescence intensity pre- and post- ATP addition. Statistics,

paired t-test; n =3 experiments, 5 embryos, 29 TCJs; p-value≤ 0.0001 (****). Violin plots show the median (dashed line) and the 25th and 75th quartiles (dotted lines).

ii. **Vinculin maintains actin and myosin patterning at tricellular junctions**

After demonstrating Vinculin's mechanosensitive recruitment to TCJs, we next turned our focus to Vinculin's relationship with the actomyosin cytoskeleton by using a Vinculin MO. First, to validate that the Vinculin knockdown (KD) was effective, we performed immunofluorescence staining on epithelia injected with either water (control) or the Vinculin MO, and we found that there is a reduction in junctional Vinculin in Vinculin KD conditions (**Figure 2A and 2B**). As Vinculin binds to actin (Bays & DeMali, 2017), we hypothesized that knocking down Vinculin would reduce the amount of actin at TCJs, and thus the amount of Myosin II, which binds to actin filaments. Epithelia were fixed and stained for F-actin (phalloidin) and Myosin II (anti-phospho-Myosin II light chain antibody). Immunofluorescence images reveal a disruption of actomyosin patterning at both bicellular junctions and TCJs (**Figures 2C and 2E**). Phalloidin intensity is reduced in the epithelia, with a specific reduction at TCJs (**Figure 2C**). Notably, we see that the characteristic "railroad track" appearance of Myosin II on either side of the junction is disrupted when Vinculin is KD (**Figure 2E**). Quantification of the fluorescence intensity of phalloidin and anti-phospho-myosin signal at TCJs revealed a strong reduction in the amount of both F-actin and Myosin II at TCJs (**Figures 2D and 2F**).

Additionally, we wanted to test the functional effects of Vinculin KD on the actin cytoskeleton at TCJs. Using optogenetic activation of RhoA again, we tested how the actin cytoskeleton responds to increased tension under both control and Vinculin KD conditions (**Figure 2G**). Based on the previous results in Figures 2A-F, we hypothesized that reduced junctional actomyosin in Vinculin KD epithelia would result in a less robust response to tension. Preliminary results show that in control epithelia, actin signal is increased, and cells exhibit a contractile response upon optogenetic stimulation. However, Vinculin KD embryos show altered apical cell area changes under increased tension: some cells experienced increased apical constriction, and others experienced apical "stretching" and had an increase in apical cell area. Additionally, when we increase tension we see F-actin "pulling away" from the TCJs

into the cytoplasm at TCJs under Vinculin KD (data not shown). Future experiments will characterize this phenotype further and allow quantification of the change in apical cell area.

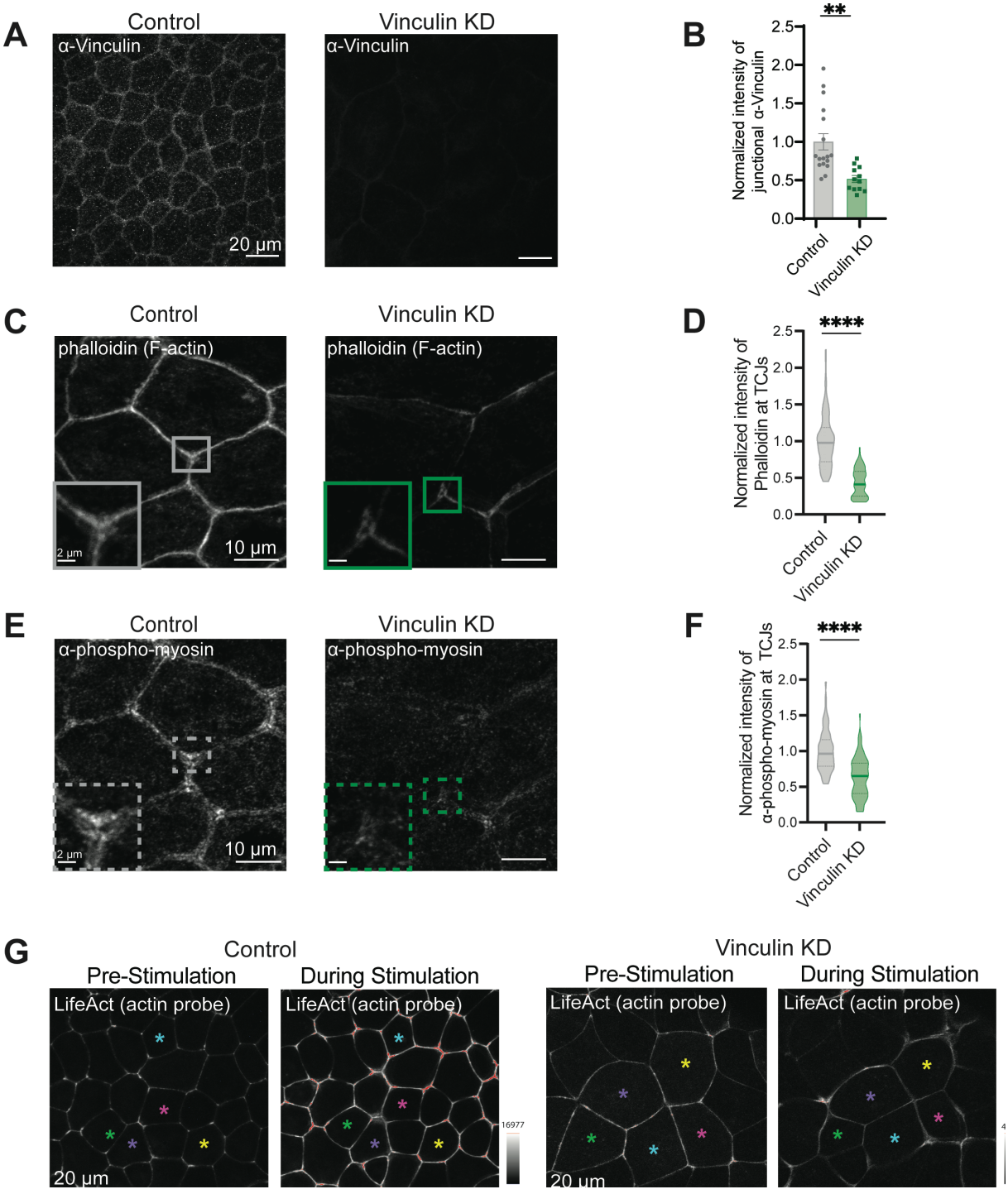

Figure 2: Vinculin maintains actin and myosin patterning at tricellular junctions.
(A) Validation of Vinculin KD through immunofluorescence staining for Vinculin in epithelia injected with either water (control) or a morpholino (Vinculin KD). **(B)** Quantification of Vinculin

immunofluorescence intensity at junctions under control and Vinculin KD conditions. Statistics, unpaired t-test; n = 2 experiments, WT = 17 embryos, Vinculin KD = 12 embryos; p-value ≤ 0.01 (**); error bars, SEMs. **(C)** *En face* view of epithelia stained for F-actin with phalloidin under control and Vinculin KD conditions. **(D)** Quantification of phalloidin (F-actin) fluorescence intensity at TCJs under control and Vinculin KD conditions. Statistics, unpaired t-test; n = 3 experiments, WT = 22 embryos and 174 TCJs, Vinculin KD = 14 embryos and 90 TCJs; p-value ≤ 0.0001 (****); error bars, SEMs. **(E)** *En face* view of epithelia immunofluorescence-stained for phosphomyosin Il under control and Vinculin KD conditions. **(F)** Quantification of phosphomyosin Il immunofluorescence intensity at TCJs under control and Vinculin KD conditions. Statistics, unpaired t-test; n = 3 experiments, WT = 22 embryos and 174 TCJs, Vinculin KD = 14 embryos and 90 TCJs; p-value ≤ 0.0001 (****); error bars, SEMs. **(G)** *En face* view of epithelia expressing the F-actin probe (LifeAct-RFP) during baseline and optogenetically-induced tension, under control and Vinculin KD conditions.

iii. **Vinculin maintains tricellular adherens and tight junctions**

Because Vinculin links AJ proteins to the cytoskeleton (Bays & DeMali, 2017), we hypothesized that Vinculin KD would affect E-cadherin signal at AJs, (as cell-cell junction specific Vinculin KD reduces cell surface E-cadherin expression (Peng et al., 2010)) and might reduce E-cadherin specifically at tAJs. To test our hypothesis, we performed immunofluorescence staining for E-cadherin in control and Vinculin KD embryos (**Figure 3A**). Vinculin KD led to a visual reduction in E-cadherin intensity (**Figure 3A**). Upon quantification of this data, we found that there is a significant reduction in E-cadherin intensity at tAJs (**Figure 3B**).

Next, to test how Vinculin maintains tTJ structure, we stained for the tTJ protein Angulin-1 because it localizes specifically to tTJs and recruits Tricellulin to these sites (Higashi et al., 2013). Using immunofluorescence staining for Angulin-1 in control and Vinculin KD embryos, we found that the levels of tTJ-specific protein Angulin-1 are reduced at TCJs under Vinculin KD conditions (**Figure 3C and 3D**).

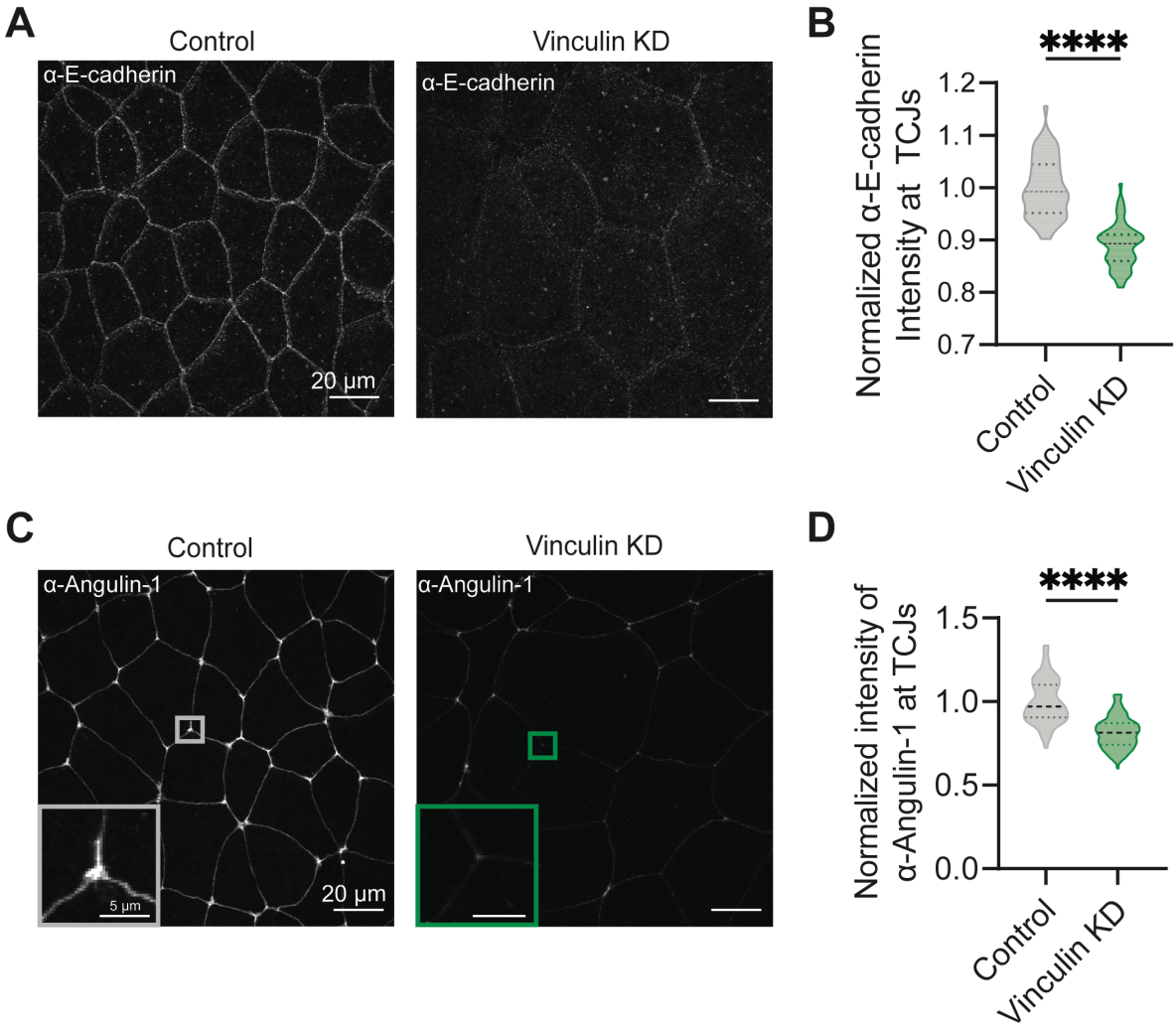

Figure 3: Vinculin maintains tricellular adherens and tight junctions.
(A) *En face* view of epithelia stained for E-cadherin under control and Vinculin KD conditions. **(B)** Quantification of E-cadherin fluorescence intensity at TCJs under control and Vinculin KD conditions. **(C)** *En face* view of epithelia stained for Angulin-1 under control and Vinculin KD conditions. **(D)** Quantification of angulin fluorescence intensity at TCJs under control and Vinculin KD conditions. Statistics, unpaired t-test with Welch's correction; n = 2 experiments, controls = 9 embryos, 20 TCJs, Vinculin KD = 7 embryos, 22 TCJs; p-value ≤ 0.0001 (****); errors bars, SEMs.

iv. **Vinculin maintains barrier function at tricellular tight junctions**

As a conclusion to this project, we wanted to test a physiological/functional aspect of Vinculin's role at TCJs. Barrier function is critical for various aspects of development and homeostasis (Marchiando et al., 2010), and tTJs are required for barrier function (Isasti-Sanchez et al., 2021). Therefore, we tested how barrier function is affected when Vinculin is KD. We used a live-imaging barrier assay developed in

our lab called ZnUMBA to measure leaks through the paracellular space (**Figure 4A**) (Higashi et al., 2022). In this assay, gastrula stage embryos are injected with a zinc indicator, FluoZin-3, and are bathed in a solution containing Zn^{2+}. When FluoZin-3 and Zn^{2+} encounter each other, FluoZin-3 fluoresces in the area in which the barrier leak occurred. When Vinculin is KD, we see an increase FluoZin-3 signal, with a specific increase at tTJs (**Figure 4B**). We quantified the number of barrier leaks at TCJs over multiple movies and found that the percentage of TCJs with barrier leaks is significantly increased when Vinculin is KD (**Figure 4C**).

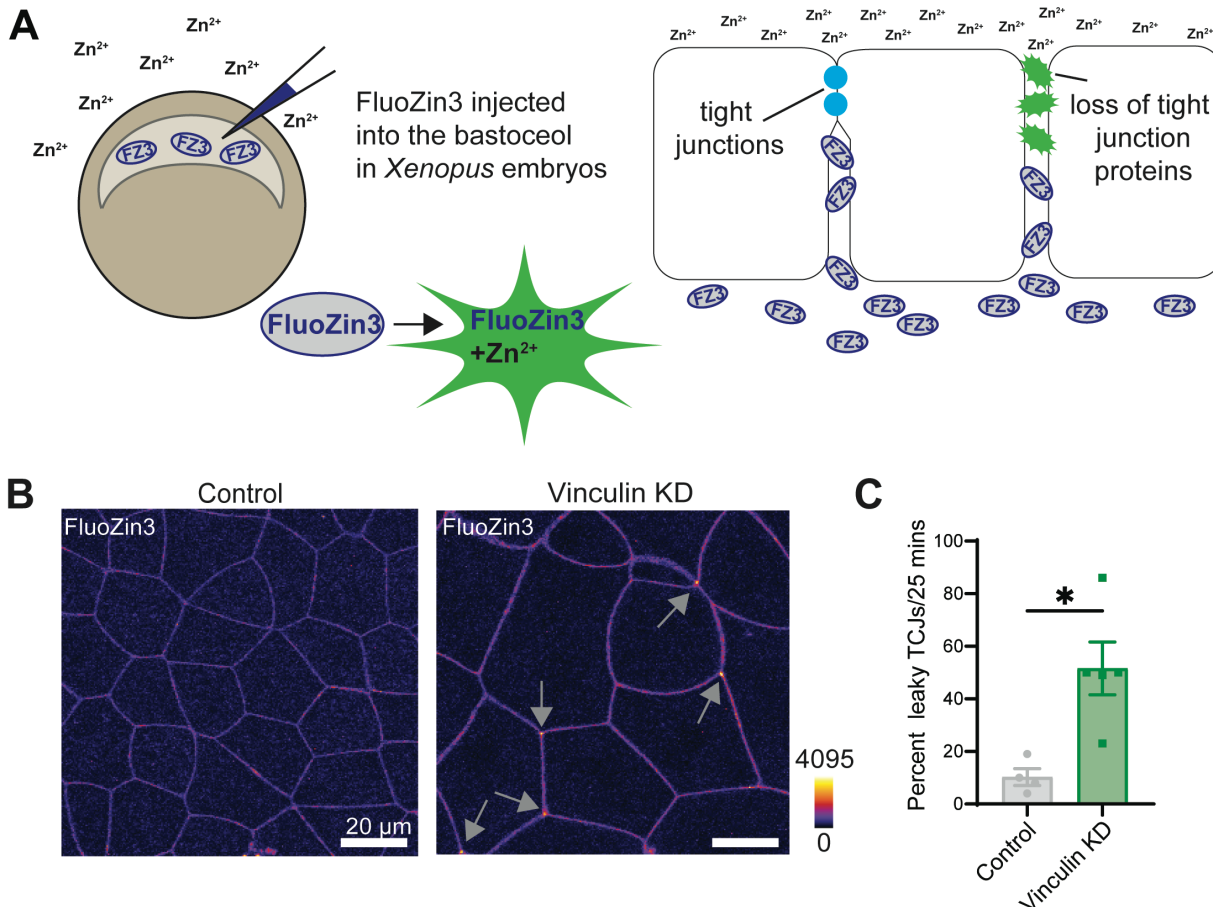

Figure 4: Vinculin maintains tricellular tight junction barrier function.
(A) Experimental setup of the ZUMBA assay. **(B)** Epithelia injected with FluoZin3 and bathed in Zn^{2+}, showing tTJ leaks in control and Vinculin KD conditions. **(C)** Quantification of frequency of tTJ leaks under control and Vinculin KD conditions. Statistics, unpaired t-test with Welch's correction; n = 3 experiments, control = 4 embryos, 223 TCJs, Vinculin KD = 5 embryos, 133 TCJs; p-value ≤ 0.05 (*); error bars, SEMs.

Discussion

i. Summary of key findings

In this study we investigated Vinculin's role at TCJs using the *X. laevis* embryonic epithelium as a model, Vinculin MO to KD the protein, immunofluorescence staining, and various live imaging techniques. First, using optogenetic activation of the small GTPase RhoA or the addition of extracellular ATP to increase tension in the epithelium, we demonstrated that fluorescently-tagged Vinculin is mechanosensitively recruited to TCJs (**Figures 1E and 1G**). To characterize Vinculin's role in tethering the actomyosin cytoskeleton to cell-cell junctions, we knocked down endogenous Vinculin using a MO (**Figures 2A and 2B**), immunofluorescence stained for F-actin and Myosin II (**Figures 2C and 2E**), and found that the intensity and organization of endogenous F-actin and Myosin II are reduced and disrupted at TCJs under Vinculin KD conditions (**Figures 2D and 2F**). Additionally, using the optogenetic activation of RhoA, our preliminary results show that the actin cytoskeleton's tension response is disrupted when Vinculin is KD (**Figure 2G**). Upon testing Vinculin's role in maintaining the AJ protein E-cadherin using immunofluorescence staining, we found that the intensity of E-cadherin is reduced at tAJs when Vinculin is KD (**Figure 3B**). Finally, we investigated Vinculin's role in upholding tTJs. We first stained for the tTJ-specific protein Angulin-1 (**Figure 3C**). Under Vinculin KD conditions, Angulin-1 intensity is significantly reduced at tTJs (**Figure 3D**). Using the ZnUMBA method developed in the Miller lab to measure barrier leaks using live imaging (**Figure 4A**), we found that there is a greater percentage of leaky tTJs when Vinculin is KD (**Figure 4C**).

Through the data collected here, we have generated an updated model of Vinculin's role at TCJs. In this model, Vinculin is present at TCJs at baseline tension and is further recruited to TCJs under increased tension. A notable deviation from previous models is that we believe Vinculin can support tTJ integrity while being an AJ protein, so we model this by adding AJ clusters with Vinculin in the TJ area (**Figure 5A**).

ii. Models of tension transmission

Previous work has detailed Vinculin's importance at focal adhesions (Atherton et al., 2016; Bays & DeMali, 2017), but less has been shown about Vinculin's role at other sites of tension transmission, like TCJs. Additionally, the ultrastructure of TCJs, the identity of the key molecular players, and the mode of actomyosin connections to these specialized cell-cell junctions is still a field of ongoing work. In their 2017 review, Higashi and Miller evaluate two models of tension transmission at TCJs: one model proposes a sarcomere-like belt of actomyosin around cell-cell junctions tethered to the tAJ through unknown proteins, whereas another proposes end-on actomyosin connections to the tAJ through linker proteins such as Vinculin and α-catenin (Higashi & Miller, 2017). The former model predicts that, upon an increase in tension, the TCJ barrier would fail and produce a gap between cells; the latter predicts that

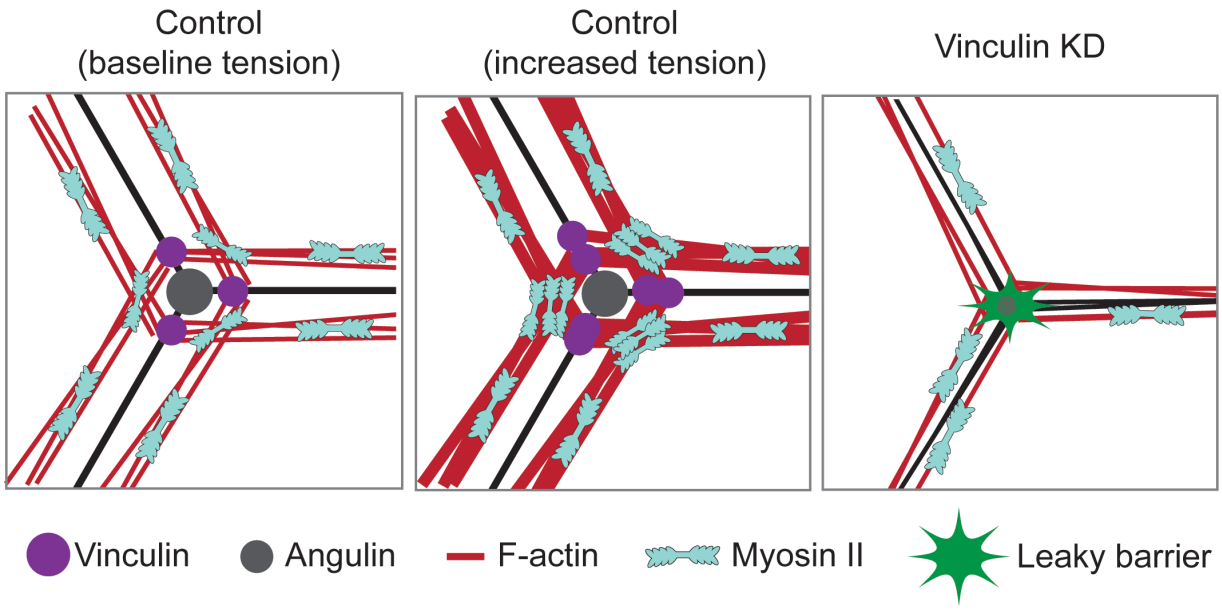

Figure 5: Proposed model of Vinculin's role at tricellular junctions showing a baseline level of Vinculin at TCJs and an increase in Vinculin under increased tension. Under Vinculin KD, the model shows decreased levels of F-actin, myosin, Angulin, and increased TCJ barrier leaks.

increased tension produces a "tightening force" that further seals the TCJ due to the recruitment of actomyosin-cytoskeleton linker proteins. Our results support the latter model. We showed that when tension is increased, fluorescently tagged Vinculin is further recruited to reinforce TCJs. Additionally, when

Vinculin is knocked down and not able to reinforce the actomyosin-TCJ connection, the "tightening force" fails and there are more frequent tTJ leaks. Further experiments characterizing actomyosin's response to increased tension at TCJs when Vinculin is KD will help us to understand the mode of actomyosin-TCJ connections.

iii. Adherens junction-tight junction interplay

Evidence has been mounting on the interdependency of AJs and TJs (Campbell et al., 2017), and this project builds on this body of work. For example, work by Cho et al. revealed that the AJ protein α-catenin binds the tTJ protein tricellulin (Cho et al., 2022). Our findings show that there is an increased percentage of tTJ leaks when Vinculin is knocked down (**Figure 4C**). This could be the result of either faulty junction development, as AJ formation is required for proper TJ formation (Campbell et al., 2017), or the result of having less Vinculin to strengthen the tAJ- and tTJ-cytoskeleton connection, as Vinculin has been shown to directly bind TJ protein ZO-1 in yeast-2-hybrid assays (Zemljic-Harpf et al., 2014). Future work involving a Vinculin construct where the region that binds ZO-1 is mutated could contribute to our understanding of whether Vinculin's ZO-1 binding ability is required for proper tTJ function and how barrier function depends on junction maintenance.

Several studies have examined Vinculin's role in barrier function. Recently, Konishi et al. found that Vinculin knockout Eph4 epithelial cells retained barrier function against larger solutes but allowed small ions to pass through the paracellular space (Konishi et al., 2019). While our work did not test paracellular permeability against large molecules, we did find that Zn^{2+} ions were allowed to pass through Vinculin KD epithelia, which we measured with fluorescence.

iv. Vinculin's role in specific tissues

As detailed above, Vinculin has an important role in epithelial cells. Interestingly, recent research has shown that Vinculin is required for proper barrier function in kidney podocytes, a specialized type of

epithelial cells that helps create a filtration barrier (Lausecker et al., 2018). Of note in this study, ZO-1 was mislocalized in podocyte-specific Vinculin knockout mice.

Vinculin has also been implicated in intercalated discs in cardiomyocytes (Merkel et al., 2019). Intercalated discs are specialized structures in cardiomyocytes that include gap junctions, desmosomes, and AJs (Vermij et al., 2017). Cardiomyocytes experience dynamic high tension due to actomyosin contractility and must maintain their cell-cell connections through such forces (Vermij et al., 2017). In cultured cardiomyocytes, Vinculin has been shown to be necessary for linking contractile myofibrils to cell-cell junctions (Merkel et al., 2019), further detailing Vinculin's important role at cell-cell junctions. While our work was not done in a cardiomyocyte model system, it contributes to our broad understanding of how Vinculin behaves in high-tension environments.

v. Conclusions and perspectives

In summary, our work shows that Vinculin is a critical component of TCJ structure and function. Furthermore, we contribute to the broader understanding of how force is transmitted between cells. Future work includes replicating optogenetically-induced increased tension in control and Vinculin KD epithelia expressing F-actin and Myosin II probes and exploring membrane-Vinculin interactions.

Materials and Methods

i. *Xenopus* handling

Adult albino and wild type *X. laevis* frogs were kept in 27L tanks and were fed and housed according to the U.S. Department of Health and Human Services Guide for the Care and Use of Laboratory Animals. Animal care and handling protocols were approved by the University of Michigan Institutional Animal Care and Use. Male wild type frogs' testes were harvested and used for egg fertilization. 2-5 days before an experiment, adult albino female frogs were primed for ovulation by injection with 50 µL human chorionic gonadotropin (HCG) and placed in a 10L tank. 1 day before an experiment, primed frogs were injected with 400-600 µL HCG to induce egg-laying.

ii. Embryo microinjections

Eggs were collected, fertilized, dejellied with 2% cysteine, and stored in 0.1X Marc's Modified Ringer's at either 13°C, 15°C, 17°C, or room temperature until microinjection to prolong desired injection stage. Embryos were microinjected 4 times at the 2- or 4-cell stage with various mRNA constructs, dye, and/or a morpholino at the following concentrations: mNeon-Vinculin, 32 pg/embryo; Halo-Vinculin, 40 pg/embryo; LifeAct-RFP, 64 pg/embryo; Janelia Fluor 646 25 µM/embryo; morpholino, 5 µM/embryo. After microinjection, embryos were allowed to develop for ~24 hours in a 15°C incubator before imaging or fixing. For ZnUMBA experiments, embryos were injected once at the gastrula stage with 10 nL of 100 µM calcium, 100 µM EDTA, and 1 mM FluoZin-3. 5 minutes post-injection, embryos were mounted in 1 mM $ZnCl_2$.

iii. DNA constructs and mRNA preparation

pCS2+/mNeon-Vinculin was generated using the forward primer 5' AAAACTCGAGAACCGGTCTTCCATACAAAG 3' and the reverse primer 5' TTTTGAATTCTCACTGGTACCATGGAGTTTTTCG 3'. These primers were used to amplify the

Vinculin insert through PCR. The Vinculin insert was cloned into the pCS2+/N-mNeon vector using restriction enzymes XhoI and EcoRI and sequence verified using Genewhiz (South Plainfield, NJ).

Additionally, several previously generated constructs were used: pCS2+/Halo-Vinculin (Dudley et al., 2022), (pCS2+/LifeAct-RFP (Higashi et al., 2016), pCS2+/prGEF-YFP (2XPDZ-YFP-LARG (DH)) (Varadarajan et al., 2022), and pCS2+/Stargazin-GFP-LOVpep (Varadarajan et al., 2022)

All constructs were transformed into Top10 competent *E. coli* cells, harvested and purified, linearized, transcribed *in vitro* with the mMessage mMachine SP6 kit (Ambion), and purified with the RNeasy kit (Qiagen).

iv. Vinculin morpholino

Vinculin morpholino (MO) targets endogenous Vinculin mRNA 5' AGCAGTTATATTCCTTATCTGAGGCACAAACCTATTGCCAAGATGCCGGTCTTC 3' in the untranslated region and was ordered from GeneTools (Philomath, OR) and diluted to a working concentration of 2.5 μM. To validate Vinculin knockdown, immunofluorescence staining for Vinculin in control and knockdown conditions was performed and junctional intensity of Vinculin signal was measured using FIJI.

v. Immunofluorescence staining and antibodies

v.i TCA Fixation:

TCA fixation was performed as following for Angulin staining: gastrula stage (Nieuwkoop and Faber stage 10-11) embryos were placed in 2% trichloroacetic acid and allowed to fix for 2 hours on a shaker, washed 3 times with phosphate-buffered saline (PBS), bisected to keep the animal cap, permeabilized with 1X PBS + 1% Triton X 100 (1% PBS-T) for 20 minutes, permeabilized with 0.1% PBS-T for 20 minutes, and blocked with 0.1% PBS-T + 5% fetal bovine serum (blocking solution) for one hour. Primary antibody was diluted for 15 minutes at 4℃ in blocking solution, bisected embryos were washed with blocking solution during this time, and diluted primary antibody was added to bisected

embryos and allowed to incubate overnight (~16 hours) at 4℃. Bisected embryos were washed with blocking solution for 5 minutes, 15 minutes, 2 hours, and overnight at 4℃. Secondary antibody was diluted in blocking solution for 15 minutes at 4℃, bisected embryos were washed with blocking solution during this time, and diluted secondary antibody was added to bisected embryos and allowed to incubate for 6 hours at 4℃. Bisected embryos were washed with blocking solution for 5 minutes, 10 minutes, 15 minutes, and overnight at 4℃. Before imaging, embryos were mounted on a slide in PBS.

v.ii. PFA fixation:

PFA fixation was performed as following for all other staining experiments: gastrula stage (Nieuwkoop and Faber stage 10-11) embryos were placed in MT Fix (1.5% paraformaldehyde, 0.25% glutaraldehyde, and 0.2 % Triton X 100 diluted in MT buffer [800 mM 1,4-Piperazinediethenaesulfonic acid, 5 mM egtazic acid, 1mM $MgCl_2$, pH to 6.8]) and allowed to fix on a shaker overnight, washed 3 times with 1X PBS, and quenched in 100 mM sodium borohydride on a shaker for 1 hour. Embryos were then washed with 1X PBS, bisected to keep the animal cap, and blocked with blocking solution B (BLANK % Tris-Buffered Saline, 10% fetal bovine serum, 5% dimethyl sulfoxide, 0.1% NP-40) overnight on a nutator at 4℃. Primary antibody was diluted for 15 minutes at 4℃ in blocking solution, bisected embryos were washed with blocking solution B during this time, and diluted primary antibody was added to bisected embryos and allowed to incubate overnight (~16 hours) at 4℃. Bisected embryos were washed 3 times in blocking solution, then for 15 minutes, and for 2 hours. Secondary antibody was diluted in blocking solution for 15 minutes at 4℃ and diluted secondary antibody was added to bisected embryos and allowed to incubate overnight at 4℃ on a nutator. After diluted secondary antibody was allowed to incubate, bisected embryos were washed 3 times in blocking solution, then washed for 15 minutes, 2 hours, and overnight at 4℃. Before imaging, embryos were mounted on a slide in PBS.

All steps were done at room temperature unless otherwise noted.

See table below for specific antibody information:

Antibody/Stain	Product Number [Company]	Species	Concentration Used
α-Angulin-1	Custom; Higashi et al. 2016	rabbit	1:50
α-E-cadherin	5D3-s [Developmental Studies Hybridoma Bank]	mouse	1:150
α-Vinculin	V9131 [Developmental Studies Hybridoma Bank]	mouse	1:400
α-ZO-1	61-7300 [Invitrogen]	rabbit	1:200
α-phosphomyosin	3671 [Cell Signal Technology]	rabbit	1:100
Alexa Fluor 488 α-mouse, or Alexa Fluor 647 α-rabbit	[Invitrogen]	goat	1:200
phalloidin-568	A12380 [Thermo Scientific]		2.5:200

vi. Microscopy

Live embryos were mounted in a chamber in a metal slide and held in place between two coverslips attached to the slide with vacuum grease. Fixed embryo animal caps were placed on a glass slide and held in place by a coverslip attached to the slide with vacuum grease.

Images were captured using an Olympus FluoView 1000 microscope with FV-10 ASV software. Images were obtained with a 60X supercorrected objective. Fixed images were acquired with a size of 512x512 pixels, an imaging speed of 10 μs/pixel, and a zoom of 1.5x. Live imaging optogenetics

videos were acquired with a size of 512x512 pixels, an imaging speed of 8 µs/pixel, and a zoom of 1.5x; live imaging ATP addition videos were acquired with a size of 256x256 pixels, an imaging speed of 10 µs/pixel, and a zoom of 3x. Live imaging ZnUMBA videos were acquired with a size of 320x320 pixels, an imaging speed of 8 µs/pixel, and a zoom of 1.5x.

vii. Quantification

All imaging acquisition parameters and post-acquisition adjustments are consistent for control and Vinculin KD conditions within an experiment, and raw data was quantified after.

vii.i ATP-induced mNeon-Vinculin recruitment to TCJ:

Videos were sum projected in FIJI, and a frame pre-ATP addition (generally between frames 0-7) and post-ATP addition (generally between frames 18-25) were chosen based on the characteristic response beginning in the embryo from LifeAct-RFP or mNeon-Vinculin signal. 6-7 distinct TCJs (distinguishable from nearby junctions) were chosen to quantify per embryo to avoid overrepresentation from any one embryo. A circular ROI size 6.62 microns in diameter was centered on the TCJs in pre- and post-ATP states, and mNeon-Vinculin integrated density signal was captured. 3 cytosolic integrated density measurements were taken per embryo and were averaged. Each tricellular integrated density measurement was divided by the average cytosolic integrated density measurement to normalize it. Normalized pre- and post-ATP addition values were divided by the average of the normalized pre-ATP addition values to set average pre-ATP addition values to one. A paired t-test was performed in GraphPad Prism for each pair of normalized tricellular integrated density measurement (pre- and post-ATP addition).

vii.ii Optogenetic-induced Halo-Vinculin recruitment to TCJ:

Videos were sum projected in FIJI, and a frame pre-stimulation (generally between frames 0-5) and during stimulation (generally between frames 14-20) were chosen based on the characteristic

response beginning in the embryo from Halo-Vinculin signal. 6-7 distinct TCJs (distinguishable from nearby junctions) were chosen to quantify per embryo to avoid overrepresentation from any one embryo. A circular ROI size 5.11 microns in diameter was centered on the TCJ in pre- and during stimulation states, and Halo-Vinculin integrated density signal was captured. 3 cytosolic integrated density measurements were taken per embryo and were averaged. Each tricellular integrated density measurement was divided by the average cytosolic integrated density measurement to normalize it. Normalized pre- and during stimulation values were divided by the average of the normalized pre-stimulation values to set average pre-stimulation values to one. A paired t-test was performed in GraphPad Prism for each pair of normalized tricellular integrated density measurement (pre- and during stimulation).

vii.iii Staining under control and Vinculin knockdown conditions:

Images were sum projected in FIJI. 6-7 distinct TCJs were chosen per embryo. A circular ROI size 6.62 microns in diameter was chosen for angulin staining experiments, and a circular ROI size 4.97 microns in diameter was chosen for actin, myosin, and E-cadherin staining experiments. The ROI was centered on a TCJ, and respective fluorescence intensity was captured through integrated density. 3 cytosolic integrated density measurements were taken per embryo and were averaged. Each tricellular integrated density measurement was divided by the average cytosolic integrated density measurement to normalize it. A t-test was performed in GraphPad Prism for normalized tricellular integrated density measurement (control and Vinculin KD conditions).

For Vinculin KD validation via staining, junctional Vinculin signal was measured by creating a mask of junctional signal in FIJI. For all images, maximum projection was used. The phalloidin channel was used to create the mask as follows: the image was duplicated to create two copies (Images A and B). A Gaussian blur with a radius of 15 was applied to Image B to remove noise. Using the image calculator, Image B was subtracted from Image A to create Image C. A Gaussian blur with a radius of 3 was applied to Image C to detect continuous junctions. Then, thresholding was applied to Image C

implementing the Huang method. The signal was then dilated one time. Any cytosolic signal in Image C was manually deleted using the poly selection tool and the image was inverted. Image C was then subjected from the maximum projection of the Vinculin channel until all cytosolic signal was removed from the Vinculin channel. The mean intensity of the Vinculin channel was then measured and recorded, and a t-test was performed in GraphPad Prism to compare control and Vinculin KD conditions.

vii.iv ZnUMBA:

All ZnUMBA videos were max projected in FIJI and the file names were coded to blind the quantification. Only videos that were at least 25 minutes long were quantified and for videos over 25 minutes, only the first 25 minutes were quantified. Criteria for leaky TCJs were as follows: a TCJ was only counted one time throughout the course of the video regardless if it leaked repeatedly or not, leaks had be at least 5 microns in diameter to be counted, the leaks had to be at TCJs (we did not count multiple cellular junctions that had 4 or more junctions intersecting), and we did not count leaks at TCJs that were at the cleavage furrow. All TCJs in a video were counted. Percent leaky TCJs was determined by dividing the number of leaky TCJs by the number of total TCJs. A t-test was performed in GraphPad Prism to compare control and Vinculin KD conditions.

viii. Figure preparation

Images were sum projected across all channels and were manually adjusted to show relevant features. A LUT was applied in FIJI. If images were differentially adjusted between control and Vinculin KD conditions, a scale bar with maximum and minimum values was added to each image.

References

Agarwal, P., & Zaidel-Bar, R. (2019). Principles of Actomyosin Regulation In Vivo. *Trends Cell Biol*, *29*(2), 150-163. https://doi.org/10.1016/j.tcb.2018.09.006

Arnold, T. R., Shawky, J. H., Stephenson, R. E., Dinshaw, K. M., Higashi, T., Huq, F., Davidson, L. A., & Miller, A. L. (2019). Anillin regulates epithelial cell mechanics by structuring the medial-apical actomyosin network. *Elife*, *8*. https://doi.org/10.7554/eLife.39065

Arnold, T. R., Stephenson, R. E., & Miller, A. L. (2017). Rho GTPases and actomyosin: Partners in regulating epithelial cell-cell junction structure and function. *Exp Cell Res*, *358*(1), 20-30. https://doi.org/10.1016/j.yexcr.2017.03.053

Atherton, P., Stutchbury, B., Jethwa, D., & Ballestrem, C. (2016). Mechanosensitive components of integrin adhesions: Role of vinculin. *Exp Cell Res*, *343*(1), 21-27. https://doi.org/10.1016/j.yexcr.2015.11.017

Barua, D., Nagel, M., & Winklbauer, R. (2021). Cell-cell contact landscapes in Xenopus gastrula tissues. *Proc Natl Acad Sci U S A*, *118*(39). https://doi.org/10.1073/pnas.2107953118

Bays, J. L., & DeMali, K. A. (2017). Vinculin in cell-cell and cell-matrix adhesions. *Cell Mol Life Sci*, *74*(16), 2999-3009. https://doi.org/10.1007/s00018-017-2511-3

Bays, J. L., Peng, X., Tolbert, C. E., Guilluy, C., Angell, A. E., Pan, Y., Superfine, R., Burridge, K., & DeMali, K. A. (2014). Vinculin phosphorylation differentially regulates mechanotransduction at cell-cell and cell-matrix adhesions. *J Cell Biol*, *205*(2), 251-263. https://doi.org/10.1083/jcb.201309092

Campbell, H. K., Maiers, J. L., & DeMali, K. A. (2017). Interplay between tight junctions & adherens junctions. *Exp Cell Res*, *358*(1), 39-44. https://doi.org/10.1016/j.yexcr.2017.03.061

Cho, Y., Haraguchi, D., Shigetomi, K., Matsuzawa, K., Uchida, S., & Ikenouchi, J. (2022). Tricellulin secures the epithelial barrier at tricellular junctions by interacting with actomyosin. *J Cell Biol*, *221*(4). https://doi.org/10.1083/jcb.202009037

Dudley, C. E., van den Goor, L., & Miller, A. L. (2022). SNAP- and Halo-tagging and dye introduction protocol for live microscopy in Xenopus embryos. *STAR Protocols*, *3*(3), 101622. https://doi.org/10.1016/j.xpro.2022.101622

Hartsock, A., & Nelson, W. J. (2008). Adherens and tight junctions: structure, function and connections to the actin cytoskeleton. *Biochim Biophys Acta*, *1778*(3), 660-669. https://doi.org/10.1016/j.bbamem.2007.07.012

Higashi, T., Arnold, T. R., Stephenson, R. E., Dinshaw, K. M., & Miller, A. L. (2016). Maintenance of the Epithelial Barrier and Remodeling of Cell-Cell Junctions during Cytokinesis. *Curr Biol*, *26*(14), 1829-1842. https://doi.org/10.1016/j.cub.2016.05.036

Higashi, T., & Miller, A. L. (2017). Tricellular junctions: how to build junctions at the TRICkiest points of epithelial cells. *Mol Biol Cell*, *28*(15), 2023-2034. https://doi.org/10.1091/mbc.E16-10-0697

Higashi, T., Stephenson, R. E., Schwayer, C., Huljev, K., Heisenberg, C.-P., Chiba, H., & Miller, A. L. (2022). Zinc-based Ultrasensitive Microscopic Barrier Assay (ZnUMBA): a live-imaging method for detecting epithelial barrier breaches with spatiotemporal precision. *bioRxiv*. https://doi.org/10.1101/2022.09.27.509705

Higashi, T., Tokuda, S., Kitajiri, S., Masuda, S., Nakamura, H., Oda, Y., & Furuse, M. (2013). Analysis of the 'angulin' proteins LSR, ILDR1 and ILDR2--tricellulin recruitment, epithelial barrier function and implication in deafness pathogenesis. *J Cell Sci*, *126*(Pt 4), 966-977. https://doi.org/10.1242/jcs.116442

Isasti-Sanchez, J., Munz-Zeise, F., Lancino, M., & Luschnig, S. (2021). Transient opening of tricellular vertices controls paracellular transport through the follicle epithelium during Drosophila oogenesis. *Dev Cell*, *56*(8), 1083-1099 e1085. https://doi.org/10.1016/j.devcel.2021.03.021

Janssen, M. E., Kim, E., Liu, H., Fujimoto, L. M., Bobkov, A., Volkmann, N., & Hanein, D. (2006). Three-dimensional structure of vinculin bound to actin filaments. *Mol Cell*, *21*(2), 271-281. https://doi.org/10.1016/j.molcel.2005.11.020

Joshi, S. D., von Dassow, M., & Davidson, L. A. (2010). Experimental control of excitable embryonic tissues: three stimuli induce rapid epithelial contraction. *Exp Cell Res*, *316*(1), 103-114. https://doi.org/10.1016/j.yexcr.2009.08.005

Kim, Y., Hazar, M., Vijayraghavan, D. S., Song, J., Jackson, T. R., Joshi, S. D., Messner, W. C., Davidson, L. A., & LeDuc, P. R. (2014). Mechanochemical actuators of embryonic epithelial contractility. *Proc Natl Acad Sci U S A*, *111*(40), 14366-14371. https://doi.org/10.1073/pnas.1405209111

Konishi, S., Yano, T., Tanaka, H., Mizuno, T., Kanoh, H., Tsukita, K., Namba, T., Tamura, A., Yonemura, S., Gotoh, S., Matsumoto, H., Hirai, T., & Tsukita, S. (2019). Vinculin is critical for the robustness of the epithelial cell sheet paracellular barrier for ions. *Life Sci Alliance*, *2*(4). https://doi.org/10.26508/lsa.201900414

Lausecker, F., Tian, X., Inoue, K., Wang, Z., Pedigo, C. E., Hassan, H., Liu, C., Zimmer, M., Jinno, S., Huckle, A. L., Hamidi, H., Ross, R. S., Zent, R., Ballestrem, C., Lennon, R., & Ishibe, S. (2018). Vinculin is required to maintain glomerular barrier integrity. *Kidney Int*, *93*(3), 643-655. https://doi.org/10.1016/j.kint.2017.09.021

Manning, L. A., Perez-Vale, K. Z., Schaefer, K. N., Sewell, M. T., & Peifer, M. (2019). The Drosophila Afadin and ZO-1 homologues Canoe and Polychaetoid act in parallel to maintain epithelial integrity when challenged by adherens junction remodeling. *Mol Biol Cell*, *30*(16), 1938-1960. https://doi.org/10.1091/mbc.E19-04-0209

Mao, Y., & Baum, B. (2015). Tug of war--the influence of opposing physical forces on epithelial cell morphology. *Dev Biol*, *401*(1), 92-102. https://doi.org/10.1016/j.ydbio.2014.12.030

Marchiando, A. M., Graham, W. V., & Turner, J. R. (2010). Epithelial barriers in homeostasis and disease. *Annu Rev Pathol*, *5*, 119-144. https://doi.org/10.1146/annurev.pathol.4.110807.092135

Mege, R. M., & Ishiyama, N. (2017). Integration of Cadherin Adhesion and Cytoskeleton at Adherens Junctions. *Cold Spring Harb Perspect Biol*, *9*(5). https://doi.org/10.1101/cshperspect.a028738

Merkel, C. D., Li, Y., Raza, Q., Stolz, D. B., & Kwiatkowski, A. V. (2019). Vinculin anchors contractile actin to the cardiomyocyte adherens junction. *Mol Biol Cell*, *30*(21), 2639-2650. https://doi.org/10.1091/mbc.E19-04-0216

Otani, T., & Furuse, M. (2020). Tight Junction Structure and Function Revisited. *Trends Cell Biol*, *30*(10), 805-817. https://doi.org/10.1016/j.tcb.2020.08.004

Peng, X., Cuff, L. E., Lawton, C. D., & DeMali, K. A. (2010). Vinculin regulates cell-surface E-cadherin expression by binding to beta-catenin. *J Cell Sci*, *123*(Pt 4), 567-577. https://doi.org/10.1242/jcs.056432

Seddiki, R., Narayana, G., Strale, P. O., Balcioglu, H. E., Peyret, G., Yao, M., Le, A. P., Teck Lim, C., Yan, J., Ladoux, B., & Mege, R. M. (2018). Force-dependent binding of vinculin to alpha-catenin regulates cell-cell contact stability and collective cell behavior. *Mol Biol Cell*, *29*(4), 380-388. https://doi.org/10.1091/mbc.E17-04-0231

Strickland, D., Lin, Y., Wagner, E., Hope, C. M., Zayner, J., Antoniou, C., Sosnick, T. R., Weiss, E. L., & Glotzer, M. (2012). TULIPs: tunable, light-controlled interacting protein tags for cell biology. *Nat Methods*, *9*(4), 379-384. https://doi.org/10.1038/nmeth.1904

Sugawara, T., Furuse, K., Otani, T., & Furuse, M. (2020). Angulin-1 seals tricellular contacts independently of tricellulin and claudins. *bioRxiv*. https://doi.org/10.1101/2020.10.02.323378

Trichas, G., Smith, A. M., White, N., Wilkins, V., Watanabe, T., Moore, A., Joyce, B., Sugnaseelan, J., Rodriguez, T. A., Kay, D., Baker, R. E., Maini, P. K., & Srinivas, S. (2012). Multi-cellular rosettes in the mouse visceral endoderm facilitate the ordered migration of anterior visceral endoderm cells. *PLoS Biol*, *10*(2), e1001256. https://doi.org/10.1371/journal.pbio.1001256

Varadarajan, S., Chumki, S. A., Stephenson, R. E., Misterovich, E. R., Wu, J. L., Dudley, C. E., Erofeev, I. S., Goryachev, A. B., & Miller, A. L. (2022). Mechanosensitive calcium flashes promote

sustained RhoA activation during tight junction remodeling. *J Cell Biol*, *221*(4). https://doi.org/10.1083/jcb.202105107

Vermij, S. H., Abriel, H., & van Veen, T. A. (2017). Refining the molecular organization of the cardiac intercalated disc. *Cardiovasc Res*, *113*(3), 259-275. https://doi.org/10.1093/cvr/cvw259

Yonemura, S. (2011a). Cadherin-actin interactions at adherens junctions. *Curr Opin Cell Biol*, *23*(5), 515-522. https://doi.org/10.1016/j.ceb.2011.07.001

Yonemura, S. (2011b). A mechanism of mechanotransduction at the cell-cell interface: emergence of alpha-catenin as the center of a force-balancing mechanism for morphogenesis in multicellular organisms. *Bioessays*, *33*(10), 732-736. https://doi.org/10.1002/bies.201100064

Yu, H. H., & Zallen, J. A. (2020). Abl and Canoe/Afadin mediate mechanotransduction at tricellular junctions. *Science*, *370*(6520). https://doi.org/10.1126/science.aba5528

Zemljic-Harpf, A. E., Godoy, J. C., Platoshyn, O., Asfaw, E. K., Busija, A. R., Domenighetti, A. A., & Ross, R. S. (2014). Vinculin directly binds zonula occludens-1 and is essential for stabilizing connexin-43-containing gap junctions in cardiac myocytes. *J Cell Sci*, *127*(Pt 5), 1104-1116. https://doi.org/10.1242/jcs.143743

Ziegler, W. H., Liddington, R. C., & Critchley, D. R. (2006). The structure and regulation of vinculin. *Trends Cell Biol*, *16*(9), 453-460. https://doi.org/10.1016/j.tcb.2006.07.004